Inorganic Chemistry

Article

pubs.acs.org/IC

Visible Light Water Oxidation Using a Co-Catalyst Loaded Anatase-Structured $Ti_{1-(5x/4)}Nb_xO_{2-y-\delta}N_y$ Compound

Tanya M. Breault, James J. Brancho, Ping Guo, and Bart M. Bartlett*

Department of Chemistry, University of Michigan, 930 North University, Ann Arbor, Michigan 48109, United States

Supporting Information

ABSTRACT: The photocatalytic activity of anatase-structured $Ti_{1-(5x/4)}Nb_xO_{2-y-\delta}N_y$ (x = 0.25, y = 0.02; NbN-25) was examined for water oxidation under UV and visible light irradiation. The semiconductor was prepared by sol–gel processing followed by nitridation in flowing ammonia and exhibits an indirect optical gap of 2.2 eV. $Ti_{1-(5x/4)}Nb_xO_{2-y-\delta}N_y$ was loaded with RuO_2 by an impregnation technique, and optimized conditions reveal that 1 wt % RuO_2 generates 16 μmol O_2 from water with concomitant IO_3^- reduction after 3 h of illumination under simulated solar radiation at a flux of 600 mW/cm^2 illumination, which corresponds to 6-sun AM1.5G illumination (compared to no detectible O_2 without the RuO_2 cocatalyst). A series of cut-on filters shows that the catalyst-loaded semiconductor evolves O_2 for $\lambda \leq 515$ nm, and a gas-phase mass spectrometry isotope labeling experiment shows that irradiating an iodate solution in $H_2{}^{18}O$ in the presence of 1 wt % RuO_2 loaded on NbN-25 gives rise to *catalytic* water oxidation: both $^{36}O_2$ and $^{34}O_2$ are observed. It is unclear whether ^{16}O arises from IO_3^- or surface reconstruction on the photocatalyst, but ICP-AES analysis of the postirradiated solution shows no dissolved metal ions.

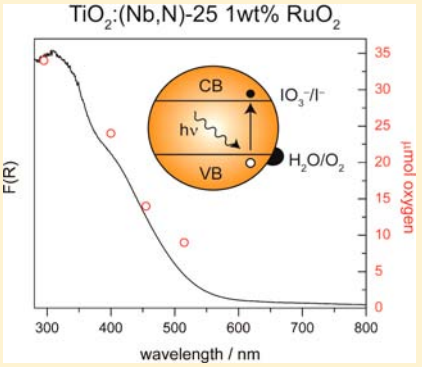

1. INTRODUCTION

Research efforts using sunlight and a photocatalyst for water splitting on a semiconducting metal oxide have been ongoing since the early 1970s with the discovery that rutile TiO_2 acts as a near-UV-active photocatalyst.[1] Titanium dioxide is an attractive material for solar to chemical energy conversion due to its abundance, low toxicity, and high photoactivity.[2] The photoactivity greatly depends on the crystalline phase and morphology, with research focusing more on anatase compared to rutile or brookite due to its higher electron mobility (4 vs. 0.1 cm^2 V^{-1} s^{-1}).[3] The positions of the conduction (Ti 3d orbitals) and valence bands (O 2p orbitals) of TiO_2 are thermodynamically suitable for both half reactions of water splitting. However, due to its large band gap (E_g > 3.1 eV, λ > 400 nm), only 5% of the solar spectrum can be efficiently used for photoconversion, which results in slow catalysis.

Current research focuses on narrow band gap oxides that absorb longer wavelengths of the solar spectrum. Narrowing the band gap of semiconductors can be achieved through various band engineering methods, typically through cation or anion incorporation, which has been reviewed extensively.[4−6] A common form of anion incorporation in oxides is the substitution of nitrogen on oxygen lattice sites (substitutional nitrogen), which is achieved synthetically through high-temperature ammonolysis. Introducing substitutional nitrogen into a metal oxide has been shown to raise the valence band edge to more negative potentials through O(2p)–N(2p) hybridization, with GaN/ZnO,[7] TaON,[8] and $LaTiO_2N$[9] emerging as promising photocatalysts for water oxidation. For these compounds, using a cocatalyst and/or sacrificial acceptor is necessary in order to observe water oxidation.

Co-alloying with charge-compensated donor–acceptor pairs in TiO_2 has also attracted attention as a promising approach to generating new visible light active photocatalysts. Research efforts, both computationally and experimentally, have focused on numerous coalloying pairs in TiO_2:(Ta,N),[10] (Nb,N),[11−13] (W,C),[14,15] and several other effective systems.[16−19] Theory predicts that stoichiometrically incorporating both a cation and an anion to balance charge results in effective hybridization with increased solubility of both the donor and the acceptor in the host structure to give materials with a smaller band gap.[20−23] Complete charge compensation between the donor and acceptor pair (a true coalloy) has yet to be fully achieved in any form of TiO_2; however, there are recent examples of photoelectrodes by Hoang et al. using (Ta,N) in rutile nanowire electrodes,[10] Cottineau et al. using (Nb,N) in mixed phase anatase/rutile nanotube electrodes,[11] and Cho et al. using (W,C) in rutile nanowire electrodes.[15] In these three reports, the coincorporated (meaning that both ions are present, but not in a charge-compensating stoichiometry) electrodes show improved photoelectrochemical response for water oxidation when compared to the singly alloyed analogues.

Our group introduced the first experimental report of incorporating both Nb^{5+} and N^{3-} in anatase TiO_2, where we targeted the high donor mole percent (25% niobium) compound, $Ti_{1-(5x/4)}Nb_xO_{2-y-\delta}N_y$, denoted as NbN-25 in this

Received: April 15, 2013
Published: July 31, 2013

   dx.doi.org/10.1021/ic400932m | Inorg. Chem. 2013, 52, 9363−9368

article. As we reported, y is only 2% in our coincoporated material. Nevertheless, we observe that methylene blue dye degrades on NbN-25 at two times the rate of commercial Degussa P25 and seven times the rate of anatase phase TiO_2.[12] In addition, we have determined the interplay between niobium loading and substitutional nitrogen in the compound. We find that high niobium mole percents are optimal for fast dye degradation due to a combination of a lower optical gap ($E_g \sim$ 2.2 eV) and a decrease in Ti^{3+} impurity states.[13] One pathway for methylene blue dye degradation using NbN-25 is the oxidation of tertiary amines to form the azure dyes. This reaction requires generating hydroxyl radicals ($^{\bullet}OH$), an active oxygen species, from aqueous solution.[24] In this article, we show that in addition to redox chemistry leading to dye degradation by active oxygen species, our champion compound, NbN-25, also acts as a visible light active water oxidation photocatalyst in the presence of a cocatalyst and an electron acceptor.

2. EXPERIMENTAL SECTION

2.1. Synthesis of $Ti_{1-(5x/4)}Nb_xO_{2-y-\delta}N_y$. All reagents were used without further purification. We have previously reported the sol−gel synthesis of the visible light absorbing semiconductor powder, NbN-25.[12] Briefly, the parent oxide $Ti_{1-(5x/4)}Nb_xO_2$ (25% niobium) was synthesized by sol−gel chemistry from $Ti(OBu)_4$ (Aldrich, 97%) and $NbCl_5$ (Strem, 99.99%). Substitutional nitrogen (N_S) was added through ammonolysis (NH_3, Cryogenic Gases, 99.99%) at 500 °C for 4 h, generating NbN-25.

An impregnation technique was used to load the desired quantity of RuO_2 cocatalyst, starting from $RuCl_3{\cdot}xH_2O$ (Strem, 99.9%). A stock solution of 1 mg/mL $RuCl_3$ was prepared by dissolving a known quantity of $RuCl_3{\cdot}xH_2O$ in Millipore water (18.2 MΩ) and stirring at room temperature. The appropriate volume of stock solution was then added to 200 mg of the photocatalyst to achieve various wt % loadings. The solutions were stirred at 100 °C until all of the water was evaporated. The cocatalyst loaded powder was subsequently annealed in the air at 350 °C for 1 h to crystallize RuO_2.

2.2. Characterization. The powders were analyzed using powder X-ray diffraction (Bruker D8 Advance diffractometer, Cu Kα radiation) with a 0.6 mm incidence slit, a step size of 0.05°/step, and a scan rate of 2 s/step. X-ray photoelectron spectroscopy was peformed using a Kratos XPS (8 mA, 14 keV, monochromatic Al source). All peaks were calibrated to the C(1s) peak at 284.5 eV. The XPS data were fit using the CasaXPS program. UV−vis spectroscopy was performed on a Cary5000 spectrophotometer (Agilent) equipped with a Praying Mantis diffuse reflectance accessory. Spectra were recorded in reflectance mode and transformed mathematically into normalized absorbance by the Kubelka−Munk function, $F(R) = (1 - R)^2/2R$. $BaSO_4$ was used as the reference material. HRTEM was performed on a JEOL 3011 TEM with a LaB_6 electron source operated at 300 kV. The samples were dispersed in methanol and drop cast onto a copper grid with an ultrathin holey carbon film (Ted Pella).

2.3. Photoelectrochemical Methods. The water oxidation reaction was performed in a custom built 64 mL Pyrex cell fit with a quartz window. A total of 50 mg of TiO_2:(Nb,N) loaded with RuO_2 was suspended in 30 mL of 1 mM $NaIO_3$ (Aldrich, >99%). The solution was purged with nitrogen for 1 h. A fluorescence probe (FOSSPOR Ocean Optics Inc.) was calibrated at 20.9% O_2 and 0% O_2 before use. Once the solution was purged and the probe equilibrated at 0% O_2, the cell was irradiated for 3 h using a Newport-Oriel 150 W Xe arc lamp fitted with appropriate filters, specified throughout. The ideal gas law was used to calculate the number of moles of O_2 produced, using the measured volume of the head space (34 mL), temperature recorded by the NeoFox probe, and partial pressure of O_2 recorded with the fluorescence probe. Henry's law was used to account for dissolved O_2. Additionally, the reaction order in the iodate anion was determined by measuring the O_2 evolution rate at various iodate concentrations (1 mM, 2 mM, and 5 mM). Control experiments were performed in a similar setup excluding cocatalyst loaded powders and iodate anions, and negligible oxygen is detected after 3 h of illumination.

2.4. Gas-Phase Mass Spectrometry. Headspace analysis of oxygen evolution experiments for isotope labeling studies were conducted using a Hiden Analytical HPR-20 mass spectrometer coupled with an Aalborg Mass Flow Controller. Helium (99.997%, Cryogenic Gases) was employed as the carrier gas. Faraday detectors were used to quantify gaseous water, helium, and nitrogen. A single-electron multiplier detector was used to quantify oxygen species ($^{32}O_2$, $^{34}O_2$, $^{36}O_2$). A custom-designed 5 mL U-shaped glass reactor equipped with a magnetic stir bar was used. In a typical experiment, 4 μL of a 0.250 M aqueous $NaIO_3$ solution was placed into the reactor, followed by evaporation of the water in a drying oven. Experiments were conducted using 6 mg of photocatalyst and 1 mL of a 1 mM $NaIO_3$ solution in either deionized water or $H_2{}^{18}O$ (Cambridge Isotope Laboratory, 97% enrichment, 99.5% purity). The solution was sparged with He for 30 min before it was attached to the mass spectrometer using Swagelok adapters. The reactor was irradiated using a Newport-Oriel 150 W Xe arc lamp at 1.2 W/cm^2, with stirring, for 1 h. The flow rate of He was 6 mL/min. To obtain the total moles of gases detected in a given experiment, the pressure data from the instrument were normalized to the flow rate of helium. The data were integrated using the flow rate at the time the lamp was activated as a baseline in Origin 8.6 to give the total volume of gas detected. The volume was then converted to moles using the ideal gas law.

2.5. Inductively Coupled Plasma/Atomic Emission Spectroscopy (ICP-AES). An ICP-AES assay was conducted on the supernatant solution from a typical oxygen evolution experiment as described in section 2.3 using the AM1.5G filter at 600 mW/cm^2 irradiance for 3 h. The solution was centrifuged on a Thermo Durafuge 100 for 10 min at 3500 rpm, and the supernatant was passed through a sintered glass frit filter funnel. The solution was then analyzed for Ti, Nb, and Ru content on a Perkin-Elmer Optima 2000DV apparatus using a Y internal standard. The emission lines used for Ti, Nb, Ru, and Y were 334.090 nm, 313.079 nm, 240.272 nm, and 371.029 nm, respectively.

3. RESULTS AND DISCUSSION

$Ti_{1-(5x/4)}Nb_xO_{2-y-\delta}N_y$ (x = 0.25) (NbN-25) was synthesized via a sol−gel route, yielding a crystalline anatase compound with an optical gap of 2.2 eV, described in a previous report.[12] An impregnation technique was used to load the RuO_2 cocatalyst by annealing at a low temperature of 350 °C to maintain substitutional nitrogen (N_S) in the compound, confirmed by X-ray photoelectron spectroscopy (Figure S1). Furthermore, at 1 wt % RuO_2 loading, the cocatalyst is not detected by X-ray diffraction. To verify that RuO_2 results from

dx.doi.org/10.1021/ic400932m | Inorg. Chem. 2013, 52, 9363−9368

the annealing treatment, a control experiment shows that annealing an aqueous solution of $RuCl_3 \cdot xH_2O$ in air at 350 °C for 1 h indeed produces polycrystalline RuO_2, confirmed by XRD (Figure S2).

High resolution transmission electron microscopy (HRTEM) images in Figure 1 show that particles have a

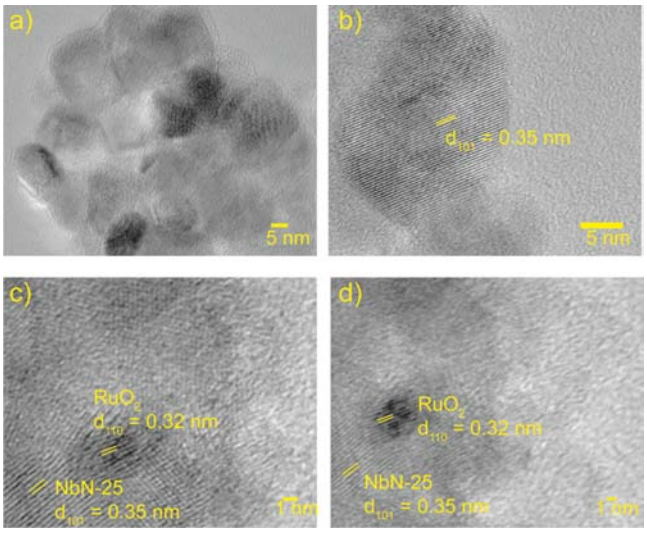

Figure 1. TEM images of (a) dispersed NbN-25 nanoparticles, (b) NbN-25 d_{101} spacing, and (c and d) 1 wt % RuO_2 loaded NbN-25.

narrow size distribution, 15 ± 5 nm, with a histogram presented in Figure S3, that aggregates. The surface area of this compound is 63 m^2/g, determined by fitting N_2 adsorption isotherms to the Brunauer–Emmett–Teller (BET) model, which supports the small particle size of ~15 nm. The NbN-25 anatase (101) lattice planes have a *d*-spacing of 0.35 nm, highlighted in Figure 1b. Figure 1c and d are representative images of NbN-25 loaded with 1 wt % RuO_2; the *d*-spacing for the (101) planes of anatase (0.35 nm) and (110) planes of RuO_2 (0.32 nm) are highlighted.

Overall water splitting (hydrogen and oxygen evolution) on semiconducting metal oxides requires large overpotentials (typically in excess of ~600 mV). Therefore, adding sacrificial donors or acceptors is often employed to evaluate either the proton reduction or water oxidation half reactions separately.[25] Our work focuses on the water oxidation reaction, and two common sacrificial electron acceptors are silver, Ag^+, and iodate, IO_3^-. Herein, we choose iodate to avoid plating metallic silver onto our particles, which then prevents maximum light absorption and decreases the rate of O_2 evolution over time.[26,27] Using iodate as a sacrificial acceptor results in the overall reaction scheme:

$$IO_3^- + 6H^+ + 6e^- \rightarrow I^- + 3H_2O \quad E^0 = 1.087V \qquad (1)$$

$$2H_2O \rightarrow 4H^+ + 4e^- + O_2 \quad E^0 = 1.23V \qquad (2)$$

$$2IO_3^- \rightarrow 2I^- + 3O_2 \quad E^0 = -0.143V \qquad (3)$$

Of note, reaction 3 is endergonic under standard conditions, and radiant energy is required to carry out the chemical reaction.

NbN-25 was tested as a water oxidation photocatalyst in 1 mM $NaIO_3$ under simulated solar irradiation (AM1.5G filter). Previous work in methylene blue dye degradation shows that oxidation products, such as benzenesulfonic acid and dimethylaniline, are derived from hydroxyl radicals and active oxygen species formed upon irradiating NbN-25.[13] However, water oxidation is not observed, suggesting that hole transfer for water oxidation is slow, and a cocatalyst that can carry out multielectron chemistry may assist in storing photogenerated holes. Under 6-sun illumination of a 1 mM $NaIO_3$ solution with 1 wt % RuO_2 loaded onto NbN-25, 15.5 μmol O_2 are observed after 3 h of irradiation, illustrated in Figure 2. A series of control

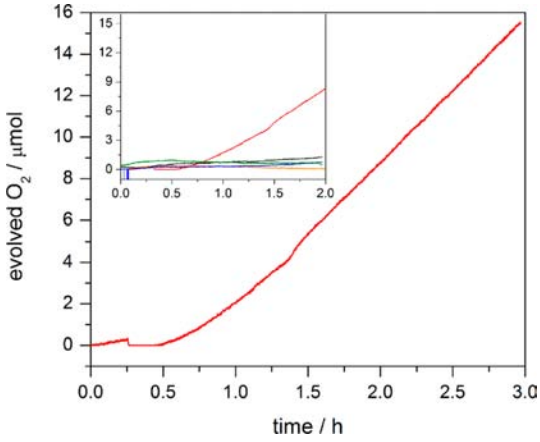

Figure 2. O_2 evolution using 50 mg of 1 wt % RuO_2 loaded NbN-25 powder, 30 mL of 1 mM $NaIO_3$, and 600 mW/cm^2 illumination by a 150 W Xe lamp, AM 1.5G filter (red). **Inset**. Control experiments (all under illumination): 1 mM IO_3^- only (black), 0.5 mg RuO_2 and 1 mM IO_3^- (blue), 1 wt % RuO_2 loaded NbN-25 (green), NbN-25 and 1 mM IO_3^- (orange).

experiments shown in the inset of Figure 2 demonstrates that only the combination of light absorber, cocatalyst, and sacrificial acceptor generate O_2 upon illumination.

The rate of the oxygen evolution reaction depends on RuO_2 loading, shown in Figure 3. The water oxidation activity improves with increasing loading percent, reaching a maximum rate at 1 wt % RuO_2. RuO_2 is required to store holes for water oxidation, as has been observed on RuO_x electrodes[28,29] and as deposited on TiO_2 powder.[30] Diffuse reflectance UV–vis spectroscopy shows that loading with 1 wt % RuO_2 does not

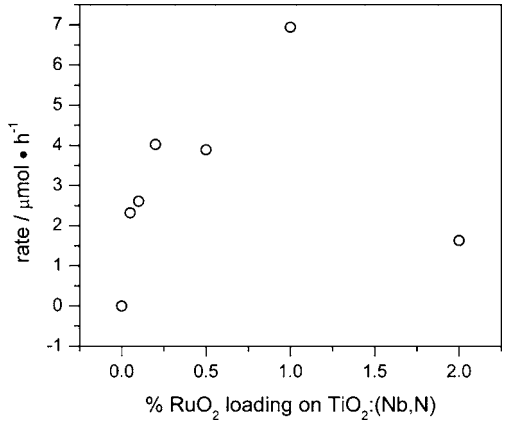

Figure 3. Optimization of RuO_2 wt % on NbN-25, annealed at 350 °C for 1 h. Reaction conditions: 50 mg of loaded powder, 30 mL of 1 mM $NaIO_3$, 600 mW/cm^2 illumination by a 150 W Xe lamp, AM 1.5G filter.

dx.doi.org/10.1021/ic400932m | *Inorg. Chem.* 2013, 52, 9363–9368

significantly alter the absorption bands of the photocatalyst (Figure S4). We hypothesize that higher RuO_2 loadings (>1%) will result in poor light absorption of NbN-25 due to the dark RuO_2 coverage on the surface of the nanoparticles, which blocks light absorption. Indeed, Figure S4 also shows that the UV−vis spectrum of particles loaded with 2 wt % RuO_2 gives a large background absorbance.

Important to establishing *photo*catalysis, we investigated the wavelength-dependent response of water oxidation on NbN-25 using a 150 W Xe lamp fitted with a water filter to eliminate IR light that can cause fluctuating temperatures upon illumination ($T = 23 \pm 3$ °C, Figure S5). The reaction conditions include 50 mg of catalyst in 30 mL of N_2-purged 1 mM $NaIO_3$ solution in an airtight cell. The cut-on filters used to probe oxygen evolution at longer wavelengths included $\lambda \geq 295$, 400, 455, and 515 nm. The irradiance for each experiment was ∼600 mW/cm^2. Figure 4a highlights that oxygen evolution tracks the

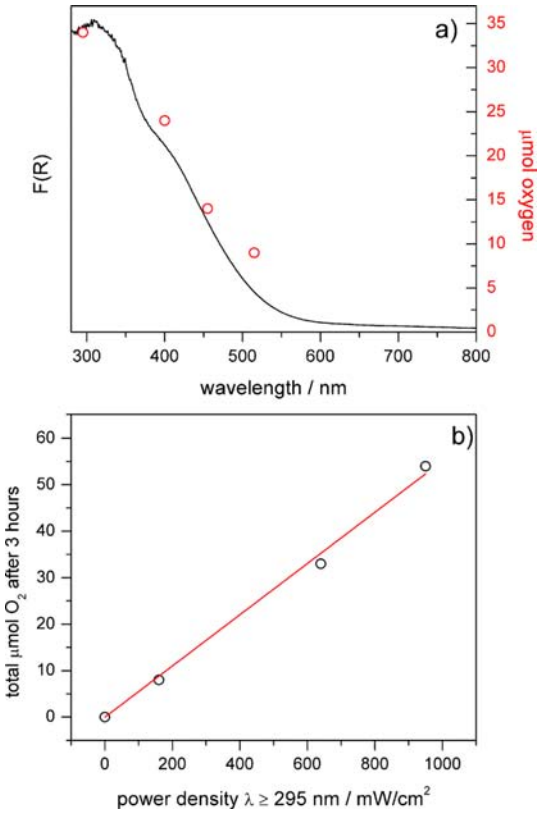

Figure 4. (a) Dependence of O_2 evolution after 3 h of irradiation with cut-on filters for NbN-25 loaded with 1 wt % RuO_2 (red). The diffuse reflectance UV−vis spectrum of NbN-25 is also shown (black). Reaction conditions: 50 mg of catalyst, 1 mM $NaIO_3$ (30 mL), 150 W Xe lamp fitted with water filter and cut-on filters, and a custom-built Pyrex cell fitted with a quartz window. (b) Oxygen evolution vs. irradiance for NbN-25 loaded with 1 wt % RuO_2. Reaction conditions: 50 mg of catalyst, 1 mM $NaIO_3$ (30 mL), 150 W Xe lamp fitted with water filter and 295 nm cut-on filter, and a custom-built Pyrex cell fitted with a quartz window.

absorption profile of the semiconductor. Although the maximum quantity of O_2 is evolved (∼33 μmol) when UV light is included ($\lambda \geq 295$), it is noteworthy that O_2 evolution persists under solely visible wavelengths. Oxygen detection at longer wavelengths suggests that the N-based impurity levels formed above the O(2p) valence band, due to both Nb^{5+} and N^{3-} in anatase TiO_2 contribute to the photocatalytic activity of this coincorporated compound for water oxidation. In addition, Figure 4b shows that the quantity of O_2 evolved after 3 h using the 295 nm cut-on filter increases linearly with irradiance, meaning that *photogenerated* charge carriers perform the redox half reactions.

In order to verify the role of iodate as a sacrificial acceptor, a series of oxygen-evolution experiments was performed as a function of IO_3^- concentration. The rate of oxygen evolution was monitored for three hours under illumination conditions described above ($\lambda \geq 295$ nm), at 1, 2, and 5 mM IO_3^-. Experiments were performed in duplicate. Figure 5 shows that

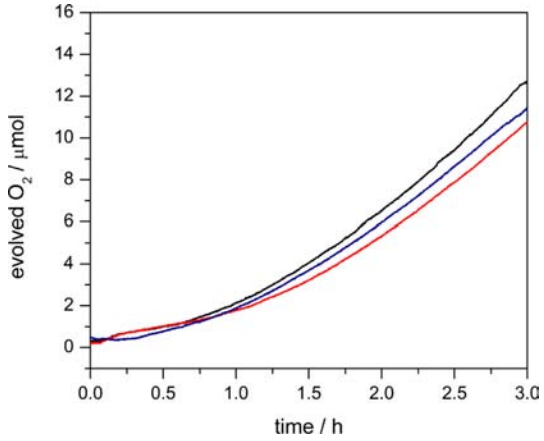

Figure 5. Oxygen evolution as a function of time for NbN-25 loaded with 1 wt % RuO_2 with different concentrations of $NaIO_3$ sacrificial acceptor. Black, red, and blue lines represent 1, 2, and 5 mM respectively.

the reaction is zero-order in IO_3^-, consistent with the generally accepted notion that, on a heterogeneous catalyst, the number of active catalytic sites is much smaller than the number of molecules of available substrate. Therefore, at practical substrate concentrations, the substrate(s) are always in excess, and the reaction is limited by poor charge carrier collection efficiency on the powdered catalyst.[31,32]

To determine the catalytic nature of the RuO_2-loaded NbN-25, oxygen-evolution experiments were carried out in isotopically labeled $H_2{}^{18}O$, and the product distribution was quantified by gas-phase mass spectrometry. We note that in all instances, there was a background signal from ambient air that could not be eliminated, which made rigorous quantification of evolved gases unreliable. However, in comparing the assays, we observe a 100-fold enhancement in the evolution of $^{34}O_2$ and a 300-fold enhancement in $^{36}O_2$ from isotopically enriched solutions, with the total oxygen evolution across all species remaining constant. The observation of $^{36}O_2$, the coupling product from oxidizing two molecules of $H_2{}^{18}O$, confirms that the RuO_2-loaded NbN-25 is indeed a photocatalytic material. However, the observed enhancement in $^{34}O_2$ is far above what would be expected statistically given the 3% abundance of $H_2{}^{16}O$ in the reactor. The result suggests that some reconstruction of the catalyst surface could be taking place along with water oxidation. Another possibility is that IO_3^- is intimately involved in the reaction mechanism both as a sacrificial electron acceptor and an O-atom donor, though not as part of the rate-determining step.

Finally, the used powder was recovered from oxygen-evolution experiments via filtration and sonicated with

dx.doi.org/10.1021/ic400932m | Inorg. Chem. 2013, 52, 9363−9368

deionized water, and dried *in vacuo*. A total of 50 mg of once-used catalyst was then added to the cell with 30 mL of 1 mM $NaIO_3$, and the oxygen-evolution rate was quantified. As seen in Figure 6, the catalyst retains only half of its activity upon

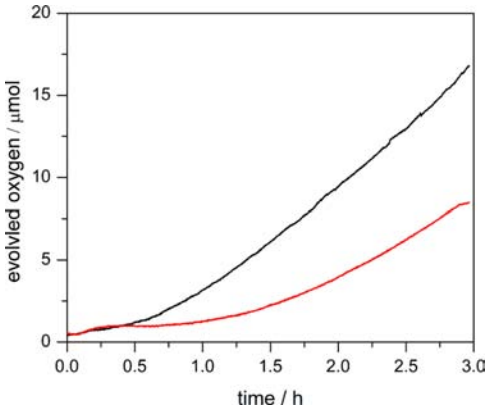

Figure 6. Oxygen evolution as a function of time for freshly prepared NbN-25 loaded with 1 wt % RuO_2 (black line) and for a second run in which the catalyst was recycled (red line). Reaction conditions: 1 mM $NaIO_3$, 600 mW/cm^2, AM 1.5G filtered light.

recycling, pointing to a loss of reactive sites either through degradation or surface passivation. Two possible degradation pathways are immediately apparent: (1) photogenerated electrons from NbN-25 can be transferred to the conduction band of RuO_2, which is lower in energy, and the Ru^{4+} reduced to soluble Ru^{3+} or Ru^{2+} and/or (2) the NbN-25 can oxidatively lose nitrogen as N_2 gas according to the reaction:[33]

$$2N^{3-} + 6h^+ \rightarrow N_2(g) \quad (4)$$

To elucidate the failure mechanism of the material, the solution was reserved after a typical oxygen-evolution experiment, centrifuged, and then filtered to remove all solid photocatalysts. The filtrate was then subjected to ICP-AES analysis. The assay reveals no detectable amounts of Ru, Ti, or Nb present in the supernatant solution after 3 h of photocatalytic oxygen evolution. This observation rules out the possibility of RuO_2 reduction. With regard to the loss of nitrogen, quantitative determination by GC/MS analysis is underway in our lab and will be reported in a future manuscript.

4. CONCLUSIONS

We report the water oxidation activity for a visible-light absorbing anatase-phase semiconductor, $Ti_{1-(5x/4)}Nb_xO_{2-y-\delta}N_y$ (NbN-25), in an aqueous $NaIO_3$ solution. NbN-25 was modified with RuO_2 by an impregnation technique, which results in polycrystalline cocatalyst loaded compounds. The cocatalyst RuO_2 is necessary in order to evolve oxygen, and water oxidation activity depends on the cocatalyst weight percent loading, with a maximum rate observed for 1 wt % RuO_2 loading. Headspace analysis experiments show that oxidizing $H_2{}^{18}O$ gives $^{36}O_2$ as a product, confirming that we are carrying out photocatalytic water oxidation on 1 wt % RuO_2-loaded NbN-25 under visible light irradiation at all absorbed wavelengths ($\lambda \leq 515$ nm).

■ ASSOCIATED CONTENT

Supporting Information

Experimental details, X-ray photoelectron spectroscopy, X-ray diffraction, UV−vis spectroscopy, histogram of particle size distribution, and oxygen evolution data. This material is available free of charge via the Internet at http://pubs.acs.org.

■ AUTHOR INFORMATION

Corresponding Author

*E-mail: bartmb@umich.edu.

Notes

The authors declare no competing financial interests.

■ ACKNOWLEDGMENTS

We thank Mr. Xiaoguang Hao for assistance with HR-TEM imaging. We thank Prof. Adam J. Matzger for use of the gas phase mass spectrometer and for useful discussions. We thank the University of Michigan for generous start-up support for instrumentation and the Rackham Graduate School for a Rackham Merit Fellowship and a Rackham One-Term Dissertation Fellowship supporting T.M.B. This work was supported by a grant from the U.S. Department of Energy, DE-FG02-11ER16262. HR-TEM and XPS instrumentation at the University of Michigan Electron Microbeam Analysis Laboratory was funded by NSF grants DMR-0315633 and DMR-0420785, respectively.

■ REFERENCES

(1) Fujishima, H.; Honda, K. *Nature* **1972**, *238*, 37−38.
(2) Chen, X.; Mao, S. S. *Chem. Rev.* **2007**, *107*, 2891−2959.
(3) Tang, H.; Prasad, K.; Sanjinès, R.; Schmid, P. E.; Lévy, F. *J. Appl. Phys.* **1994**, *75*, 2042−2047.
(4) Rehman, S.; Ullah, R.; Butt, A. M.; Gohar, N. D. *J. Hazard. Mater.* **2009**, *170*, 560−569.
(5) Palaez, M.; Nolan, N. T.; Pillai, S. C.; Seery, M. K.; Falaras, P.; Kontos, A. G.; Dunlop, P. S. M.; Hamilton, J. W. J.; Byrne, J. A.; O'Shea, K.; Entezari, M. H.; Dionysiou, D. D. *Appl. Catal, B.: Environ.* **2012**, *125*, 331−349.
(6) Augustynski, J.; Alexander, B. D.; Solarksa, R. *Top. Curr. Chem.* **2011**, *303*, 1−38.
(7) Maeda, K.; Takata, T.; Hara, M.; Saito, N.; Inoue, Y.; Kobayashi, H.; Domen, K. *J. Am. Chem. Soc.* **2005**, *127*, 8286−8287.
(8) Hitoki, G.; Takata, T.; Kondo, J.; Hara, M.; Kobayashi, H.; Domen, K. *Chem. Commun.* **2002**, 1698−1699.
(9) Kasahara, A.; Nukumizu, K.; Hitoki, G.; Takata, T.; Kondo, J. N.; Hara, M.; Kobayashi, H.; Domen, K. *J. Phys. Chem. A* **2002**, *106*, 6750−6753.
(10) Hoang, S.; Guo, S.; Mullins, C. B. *J. Phys. Chem. C* **2012**, *116*, 23283−23290.
(11) Cottineau, T.; Béalu, N.; Gross, P.-A.; Pronkin, S. N.; Keller, N.; Savinova, E. R.; Keller, V. J. *Mater. Chem. A* **2013**, *1*, 2151−2160.
(12) Breault, T. M.; Bartlett, B. M. *J. Phys. Chem. C* **2012**, *116*, 5986−5994.
(13) Breault, T. M.; Bartlett, B. M. *J. Phys. Chem. C* **2013**, *117*, 8611−8618.
(14) Neville, E. M.; Mattle, M. J.; Loughrey, D.; Rajesh, B.; Rahman, M.; MacElroy, J. M. D.; Sullivan, J. A.; Thampi, K. R. *J. Phys. Chem. C* **2012**, *116*, 16511−16521.
(15) Cho, I. S.; Lee, C. H.; Feng, Y.; Logar, M.; Rao, P. M.; Cai, L.; Kim, D. R.; Sinclair, R.; Zheng, X. *Nature Commun.* **2013**, *4*, 1723/1−8.
(16) Liu, G.; Zhao, Y.; Sun, C.; Li, F.; Lu, G. Q.; Cheng, H.-M. *Angew. Chem., Int. Ed.* **2008**, *47* (24), 4516−4520.
(17) Chen, D.; Jiang, Z.; Geng, J.; Wang, Q.; Yang, D. *Ind. Eng. Chem. Res.* **2007**, *46* (9), 2741−2746.

(18) Hoang, S.; Berglund, S. P..; Hahn, N. T.; Bard, A. J.; Mullins, C. B. *J. Am. Chem. Soc.* **2012**, *134* (8), 3659−3662.
(19) Etacheri, V.; Seery, M. K.; Hinder, S. J.; Pillai, S. C. *Inorg. Chem.* **2012**, *51* (13), 7164−7173.
(20) Ma, X.; Wu, Y.; Lu, Y.; Xu, J.; Wang, Y.; Zhu, Y. *J. Phys. Chem. C* **2011**, *115*, 16963−16969.
(21) Yin, W.-J.; Tang, H.; Wei, S.-H.; Al-Jassim, M. M.; Turner, J.; Yan, Y. *Phys. Rev. B* **2010**, *82*, 045106/1−6.
(22) Wan, D.; Zou, Y.; Wen, S.; Fan, D. *Appl. Phys. Lett.* **2009**, *95*, 012106/1−3.
(23) Gai, Y.; Li, J.; Li, S.-S.; Xia, J.-B.; Wei, S.-H. *Phys. Rev. Lett.* **2009**, *102*, 036402.
(24) Konstantinou, I. K.; Albanis, T. A. *Appl. Catal. B: Environ.* **2004**, *49*, 1−14.
(25) Abe, R.; Higashi, M.; Domen, K. *Chem. Sus. Chem.* **2011**, *4*, 228−237.
(26) Maeda, K.; Shimodaira, Y.; Lee, B.; Teramura, K.; Lu, D.; Kobayashi, H.; Domen, K. *J. Phys. Chem. C* **2007**, *111*, 18264−18270.
(27) Chen, S.; Yang, J.; Ding, C.; Li, R.; Jin, S.; Wang, D.; Han, H.; Zhang, F.; Li, C. *J. Mater. Chem. A* **2013**, DOI: 10.1039/c3ta10446j.
(28) Lodi, G.; Sivieri, E.; De Battisti, A.; Trasatti, S. *J. Appl. Electrochem.* **1978**, *8*, 135−143.
(29) Näslund, L.-Å.; Sánchez-Sánchez, C. M.; Ingason, Á. S.; Bäckström, J.; Herrero, E.; Rosen, J.; Holmin, S. *J. Phys. Chem. C* **2013**, *117*, 6126−6135.
(30) Borgarello, E.; Pelizzetti, E. *Inorg. Chim. Acta* **1984**, *91*, 295−300.
(31) Kudo, A.; Miseki, Y. *Chem. Soc. Rev.* **2009**, *38*, 253−278.
(32) Linsebigler, A. L.; Lu, G.; Yates, J. T., Jr. *Chem. Rev.* **1995**, *95*, 735−758.
(33) Hitoki, G.; Takata, T.; Kondo, J. N.; Hara, M.; Kobayashi, H.; Domen, K. *Chem. Commun.* **2002**, *16*, 1698−1699.